extent of the charge density shift, since an observable difference is not seen between the two systems.

Charge density shifts are often assumed for other mixed Mo–W complexes in order to explain some of their abnormal properties.[11,17,19,23] A typical example is observed for dinuclear complexes with quadruple metal–metal bonds.[19] The ^{31}P NMR chemical shifts for the coordinated phosphines, for example, only show very small differences between the two homonuclear metal complexes $Mo_2(PR_3)_4Cl_4$ and $W_2(PR_3)_4Cl_4$. The difference, however, is remarkably large between the two kinds of ^{31}P chemical shifts in the mixed-metal complex. Such a remarkable change in the chemical shift is not observed for the ^1H and ^{13}C NMR spectra of our system. This is probably related to the distance of the ^1H and ^{13}C nuclei from the metal centers and also to the possibly small degree of the charge density shift in the present complexes.

The electronic structure of $[Mo_2(O)_2(\mu\text{-}O)_2(R\text{-cys})_2]^{2-}$ (*R*-cys = (*R*)-cysteinate(2-) ion) has been calculated by the all-valence-electron SCF MO method, and the absorption peaks in the region >250 nm have been claimed to be due to the transitions from the orbital with essentially Mo–Mo σ-bonding character to higher Mo–Mo bonding and antibonding orbitals.[59] Such a result is virtually unaffected by the difference in chelate ligands coordinated to the dimeric unit. Since the correspondence of the absorption peaks of the three Mo_2, MoW, and W_2 complexes is reasonably good, the absorption bands at >250 nm of the MoW and W_2 complexes should also be due to the transitions involving the metal–metal molecular orbitals. Thus, the electronic interaction between the two different metal ions, Mo and W, should not be significantly different in nature from those of the two homonuclear complexes. The oxidation potential of the MoW complex is between those of the two homonuclear complexes. An electron should, therefore, be removed from the Mo–W σ-bonding orbital rather than from an orbital localized on one of the metal centers.

Acknowledgment. The XPS spectra were obtained under the joint research program with the Institute for Molecular Science (1986-1987). We thank Dr. Y. Nakamura (Tokyo Institute of Technology) for ^{95}Mo and ^{183}W NMR measurements and Dr. M. Ebihara and T. Yamaguchi for the crystal structure determination.

Supplementary Material Available: Figure S1, showing a stereoscopic view of the crystal structure of $Na_2[MoW(O)_2(\mu\text{-}O)_2(edta)]\cdot 4.5H_2O$, and Tables SI, SII, SIV, and SV, listing details of the reflection data collection, anisotropic thermal parameters, bond distances, and bond angles (8 pages); Table SIII, listing calculated and observed structure factors (6 pages). Ordering information is given on any current masthead page.

(59) Brown, D. H.; Perkins, P. G.; Stewart, J. J. *J. Chem. Soc., Dalton Trans.* **1972**, 1105-1108.

Contribution from the Department of Chemistry, University of Houston, Houston, Texas 77204-5641

Synthesis, Molecular Structure, and Electrochemical Properties of Two Geometric Isomers of Tetrakis(μ-2-anilinopyridinato)dirhodium Complexes

J. L. Bear,* C.-L. Yao, L.-M. Liu, F. J. Capdevielle, J. D. Korp, T. A. Albright, S.-K. Kang, and K. M. Kadish*

Received August 31, 1988

Two geometric isomers of the tetrakis(μ-2-anilinopyridinato)dirhodium unit, $[Rh_2(ap)_4]^{n+}$ (n = 0, 1), were synthesized by using different preparative procedures. Crystal and molecular structures were determined by single-crystal X-ray diffraction and show one complex, $Rh_2(ap)_4(NCC_6H_5)$ (**1b**), to have two pyridyl and two anilino nitrogens bound to each rhodium atom trans to their own kind and to have one axially bound benzonitrile. The second complex, $Rh_2(ap)_4Cl$ (**2a**), has four pyridyl nitrogens and one chloride ion bound to one rhodium atom and has four anilino nitrogens bound to the other rhodium atom. Compound **1b**, $C_{51}H_{41}N_9Rh_2$, crystallizes in the orthorhombic space group *Pbca* with eight formula weights in a unit cell of dimensions a = 21.002 (7) Å, b = 17.317 (6) Å, and c = 26.028 (8) Å and refined to R = 0.063. Compound **2a**, $C_{44}H_{36}N_8ClRh_2$, crystallizes in the monoclinic space group $I2/c$ with four formula weights in a unit cell having dimensions a = 20.321 (5) Å, b = 9.594 (2) Å, c = 21.273 (4) Å, and β = 111.35 (2)°, with final R = 0.031. Compound **1** (**1b** without axial benzonitrile) undergoes two reversible one-electron oxidations in CH_2Cl_2, 0.1 M TBAP, at 0.08 and 0.82 V vs SCE. Complex **2a** is reversibly reduced by one electron at -0.38 V and reversibly oxidized by one electron at 0.52 V in CH_2Cl_2. Electrochemical studies show that compound **1a** (singly oxidized **1**) forms bisadducts of Cl^-, CN^-, or CH_3CN in CH_2Cl_2 solutions containing high concentrations of these ligands whereas **2a** exists only as a monoadduct. The ESR spectra of **1a** (rhombic signal with g_3 split into a 1:2:1 triplet) and **2a** (axial signal with $g_\parallel$ split into a doublet) are consistent with the singly occupied molecular orbital (SOMO) being equally distributed on both Rh atoms in the former complex and being localized on one rhodium atom in the latter. Extended Hückel calculations were carried out on $[Rh_2(O_2CH)_4]^+$, $[Rh_2((NH)_2CH)_4]^+$, and $[Rh_2((NH)_2CH)_4(L)]^+$, and the mechanisms for localization of the odd electron on **2a** are discussed.

Introduction

The synthesis and spectroelectrochemical characterization of a dinuclear rhodium complex containing four 2-anilinopyridinate ligands (ap) were first reported by Tocher and Tocher.[1] The orientation of the bridging 2-anilinopyridinate ions was not determined for the reported complex, and it was not known which of the four possible geometric isomers was synthesized. Our laboratory was successful in obtaining two geometric forms of the tetrabridged complex, and we reported preliminary results on the structure, electrochemistry, and ESR properties of these species.[2] One of the two isomers has a (2,2-trans) donor atom arrangement, which consists of two pyridyl (N_p) and two anilino (N_a) nitrogens on each rhodium atom bound trans to their own kind (compound **1**). The other isomer (compound **2**) has a (4,0) arrangement with four pyridyl nitrogens bound to one rhodium atom and four anilino nitrogens bound to the other rhodium atom.

The different bonding arrangement of the pyridyl and anilino nitrogens has a significant effect on the UV–vis and ESR spectra of the two isomeric forms. The singly oxidized form of compound **1** (called compound **1a**) has a rhombic ESR signal with g_3 split into a 1:2:1 triplet, whereas the radical cation of **2** (called compound **2a**) shows an axial signal with $g_\parallel$ split into a doublet. These results are consistent with the spin density of the odd electron being distributed equally on both rhodium ions in the former complex

(1) Tocher, D. A.; Tocher, J. L. *Inorg. Chim. Acta* **1985**, *104*, L15.
(2) Bear, J. L.; Liu, L.-M.; Kadish, K. M. *Inorg. Chem.* **1987**, *26*, 2927.

0020-1669/89/1328-1254$01.50/0

and localized on one rhodium ion in the latter complex.

A polarization of the odd-electron spin density in $Rh^{II}Rh^{III}$ complexes is not exclusively due to different bonding arrangements of hetero donor atom bridging ligands. The ESR spectrum of $[Rh_2(dpb)_4]^+$, where dpb = *N,N'*-diphenylbenzamidinate ion, has been reported[3] and in acetonitrile has a $g_\parallel$ that is split into a doublet of doublets rather than a 1:2:1 triplet. This result is unexpected, since both rhodium ions in this complex have identical equatorial ligand environments. When the ESR spectrum of the radical cation is recorded in the nonbonding solvent CH_2Cl_2, a 1:2:1 triplet is observed for $g_\parallel$. It was suggested that only the CH_3CN monoadduct of $[Rh_2(dpb)_4]^+$ exists in CH_3CN solutions and that the bonding of CH_3CN to only one rhodium atom increases the spin density of the unpaired electron on the rhodium that does not contain an axial ligand.[3] Likewise in $[Rh_2(form)_4]^+$ (form = *N,N'-p*-tolylformamidinate), $g_\parallel$ is split into a 1:2:1 triplet, whereas the CO monoadduct exhibits a doublet of doublets.[4]

The degree of polarization of the odd-electron orbital observed in $Rh_2(ap)_4Cl$ (**2a**) is unprecedented for dirhodium complexes and raises questions regarding the factors that lead to localization of the unpaired electron on one of the two rhodium atoms. It is also reasonable that if the singly occupied orbital of the oxidized complex **2a** is primarily centered on one rhodium ion, then **2**, which has two electrons in this orbital, should behave much like a mixed-valent Rh^IRh^{III} complex. This may account for the large differences in the redox potentials of the two geometric isomers[2] and the propensity of the complex to form only monoadducts.

In this paper we present the syntheses, detailed descriptions of structures, and data on the chemical and electrochemical properties of the two complexes.

Experimental Section

Chemicals. $RhCl_3 \cdot 3H_2O$ was obtained from Alfa Inorganics and used to prepare $Rh_2(OOCCH_3)_4$ by a literature method.[5] The ligand 2-anilinopyridine was purchased from Aldrich and recrystallized from hexane. Tetra-*n*-butylammonium perchlorate (TBAP, Fluka Chemicals) was recrystallized twice from ethanol and used as supporting electrolyte. All solvents were of reagent grade and were purified by standard procedures before use.

Preparation of $Rh_2(ap)_4$ (1). Compound **1** was prepared by the method described by Tocher and Tocher,[1] which involves the reaction of 0.5 g of $RhCl_3 \cdot 3H_2O$ with an excess of the sodium salt of 2-anilinopyridine in refluxing ethanol. The yield is 22% after recrystallization from CH_2Cl_2/hexane.

Preparation of $Rh_2(ap)_4Cl$ (2a). Compound **2a** was synthesized by heating 100 mg of $Rh_2(O_2CCH_3)_4$ and 6 g of 2-anilinopyridine in a 50-mL round-bottom flask at 130 °C for 20 h under vacuum. At the end of the 20-h period, excess 2-anilinopyridine was removed by sublimation. The remaining mixture was dissolved in CH_2Cl_2 containing 10% (v/v) CCl_4, and the solution was placed on a silica gel column and eluted with a 5%:95% ethanol:methylene chloride solution. The red band was collected and the solvent removed. The red solid was recrystallized from a mixture of CH_2Cl_2 and CH_3CN. A 40% yield of **2a** was obtained.

It should be pointed out that none of the reactants contain the chloride ion, and yet the product contains an axial chloride. The chloride ion results from one or both of the following reactions: (1) thermal or photochemical electron transfer from **2** to CCl_4, which undergoes dissociative electron capture, or (2) the reaction of **2** with dioxygen to form the superoxide complex $Rh_2(ap)_4O_2$, which reacts with CCl_4 or CH_2Cl_2 to abstract the chloride. Both electron-transfer processes described in (1) have been shown to occur in our laboratory, and the reaction of superoxide with chlorocarbons is documented in the literature.[6]

Instrumentation. ESR spectra were measured on a Bruker Model 100D ESR spectrometer. Cyclic voltammetric measurements were carried out on an IBM EC 225 voltammetric analyzer utilizing a three-electrode configuration. The working electrode consisted of a platinum button with a surface area of 0.19 mm^2. A saturated calomel electrode (SCE) was used as the reference electrode. For controlled-potential coulometry, a BAS Model SP-2 synthetic potentiostat was used. A Perkin-Elmer Model 330 spectrometer was used to record electronic absorption spectra. The CO adducts of the dirhodium compounds were incorporated into CsI pellets, and the infrared spectra were measured on a Perkin-Elmer Model 1330 spectrometer.

Table I. X-ray Data Collection and Processing Parameters

	1b	**2a**
space group	*Pbca*	*I2/c*
cell constants		
a, Å	21.002 (7)	20.321 (5)
b, Å	17.317 (6)	9.594 (2)
c, Å	26.028 (8)	21.273 (4)
β, deg		111.35 (2)
V, Å^3	9466	3863
chem formula	$Rh_2C_{51}H_{41}N_9$	$Rh_2C_{44}H_{36}N_8Cl$
fw	985.77	918.09
formula units/cell, *Z*	8	4
density (calc), g/cm^3	1.38	1.58
abs coeff, cm^{-1}	7.28	9.53
λ(Mo Kα), Å	0.71073	0.71073
$R(F_o)$	0.063	0.031
$R_w(F_o)$	0.074	0.028

X-ray Data Collection and Processing. It was difficult to obtain a crystal of **1** that was stable in the X-ray beam long enough for X-ray analysis. A suitable crystal was finally obtained from a CH_2Cl_2 solution containing a small amount of benzonitrile. An extremely thin black-purple plate of **1b** (**1b** is **1** with one axially bound benzonitrile) having dimensions 0.50 × 0.50 × 0.04 mm was mounted on a glass fiber in a random orientation on an Enraf-Nonius CAD-4 automatic diffractometer. The radiation used was Mo Kα monochromatized by a dense graphite crystal assumed for all purposes to be 50% imperfect. Crystallographic data are listed in Table I. The Laue symmetry was determined to be *mmm*, and from the systematic absences noted, the space group was shown unambiguously to be *Pbca*. Intensities were measured by using the θ–2θ scan technique, with the scan rate depending on the net count obtained in rapid prescans of each reflection. Two standard reflections were monitored periodically during the course of the data collection as a check of crystal stability and electronic reliability, and these did not vary significantly. In reducing the data, Lorentz and polarization factors were applied, but no correction for absorption was made due to the small absorption coefficient. Unfortunately, the size of the crystal prevented more data from being collected.

The structure was solved by MULTAN, which revealed the positions of both rhodium atoms in the asymmetric unit consisting of one full molecule. The remaining non-hydrogen atoms were found in difference Fourier syntheses, which showed the molecule to be in the trans configuration. Due to the relatively small amount of observed data, only the rhodium atoms were refined anisotropically. All hydrogens were entered in ideally calculated positions and held fixed. After all shift/esd ratios were less than 0.2, convergence was reached at the agreement factors listed in Table I. No unusually high correlations were noted between any of the variables in the last cycle of least-squares refinement, and the final difference density map showed no peaks greater than 0.80 e/Å^3. All calculations were made by using the Molecular Structure Corp. TEXRAY 230 modifications of the SDP-PLUS series of programs.

A very small dark burgundy plate of **2a** with approximate dimensions 0.25 × 0.25 × 0.10 mm was mounted on a glass fiber in a random orientation. Crystallographic data are also listed in Table I. The Laue symmetry was determined to be $2/m$, and from systematic absences noted, the space group was shown to be either *Ic* or *I2/c*. The conventional setting *C2/c* (or *Cc*) was not used in this case, since this would have a β angle much further from 90° (the *C*-centered cell has a = 23.47 Å, b = 9.59 Å, c = 21.27 Å, and β = 126.2°). All other procedures and methods used for structure determination were the same as described for **1b**. The asymmetric unit comprises only one-half molecule situated on a 2-fold axis that passes through the Rh and Cl atoms. Non-hydrogen atoms were refined anisotropically, and hydrogen atoms were positioned ideally.

Computation Details. The extended Hückel calculations[7] used a modified Wolfberg–Helmholz formula.[8] The atomic parameters were taken from previous work. The geometries for $Rh_2(O_2CH)_4$ and $Rh_2((NH)_2CH)_4$ were taken from the literature.[9,10] In the acetonitrile

(3) Le, J. C.; Chavan, M. Y.; Bear, J. L.; Kadish, K. M. *J. Am. Chem. Soc.* **1985**, *107*, 7195.
(4) Piraino, P.; Bruno, G.; Lo Schaivo, S.; Laschi, F.; Zanello, P. *Inorg. Chem.* **1987**, *26*, 2205.
(5) Rampel, G. A.; Legzdin, P.; Smith, H.; Wilkinson, G. *Inorg. Synth.* **1972**, *13*, 90.
(6) Bear, J. L.; Yao, C.-L; Capdevielle, F. J.; Kadish, K. M. *Inorg. Chem.* **1988**, *27*, 3782.
(7) Hoffmann, R. *J. Chem. Phys.* **1963**, *39*, 1397. Hoffmann, R.; Lipscomb, W. N. *Ibid.* **1962**, *36*, 2179; **1962**, *37*, 2872.
(8) Ammeter, J. H.; Burgi, H.-B.; Thibeault, J. C.; Hoffmann, R. *J. Am. Chem. Soc.* **1977**, *99*, 7546.
(9) Summerville, R. H.; Hoffmann, R. *J. Am. Chem. Soc.* **1976**, *98*, 7240.

Table II. Selected Bond Lengths (Å) and Angles (deg)

length	1b	2a	angle	1b	2a
Rh(1)–Rh(2)	2.412 (1)	2.406 (1)	Rh–Rh–L(ax)	178.5 (2)	180.00
Rh–N(1)	2.042 (9)	2.045 (3)	Rh–Rh–N(1)	88.0 (3)	86.7 (1)
Rh–N(2)	2.043 (7)	2.009 (4)	Rh–Rh–N(2)	87.2 (2)	86.7 (1)
Rh–N(3)	2.051 (8)	2.052 (3)	Rh–Rh–N(3)	86.7 (2)	86.4 (2)
Rh–N(4)	2.016 (8)	2.008 (3)	Rh–Rh–N(4)	88.0 (3)	87.3 (1)
Rh–N(5)	2.035 (9)		Rh–Rh–N(5)	90.0 (3)	
Rh–N(6)	2.084 (9)		Rh–Rh–N(6)	85.4 (3)	
Rh–N(7)	2.013 (9)		Rh–Rh–N(7)	86.1 (3)	
Rh–N(8)	2.022 (9)		Rh–Rh–N(8)	88.4 (3)	
Rh–L(ax)	2.189 (10)	2.421 (3)	Rh–N(1)–C(5)	121.5 (8)	118.3 (3)
N(1)–C(1)	1.36 (1)	1.359 (6)	Rh–N(2)–C(5)	123.9 (7)	120.1 (3)
N(1)–C(5)	1.38 (1)	1.362 (6)	Rh–N(2)–C(6)	119.6 (6)	120.0 (3)
N(2)–C(5)	1.35 (1)	1.348 (6)	C(5)–N(2)–C(6)	116.4 (9)	119.9 (4)
N(2)–C(6)	1.46 (1)	1.419 (6)	Rh–N(3)–C(16)	119.8 (7)	118.8 (3)
N(3)–C(12)	1.39 (1)	1.367 (6)	Rh–N(4)–C(16)	124.0 (8)	119.3 (3)
N(3)–C(16)	1.41 (1)	1.366 (6)	Rh–N(4)–C(17)	116.4 (7)	120.6 (3)
N(4)–C(16)	1.30 (1)	1.355 (6)	C(16)–N(4)–C(17)	117.0 (10)	120.1 (4)
N(4)–C(17)	1.42 (1)	1.406 (5)	Rh–N(5)–C(27)	120.1 (8)	
N(5)–C(23)	1.31 (1)		Rh–N(6)–C(27)	123.0 (8)	
N(5)–C(27)	1.32 (1)		Rh–N(6)–C(28)	113.4 (7)	
N(6)–C(27)	1.35 (1)		C(27)–N(6)–C(28)	122.4 (9)	
N(6)–C(28)	1.48 (1)		Rh–N(7)–C(38)	122.6 (8)	
N(7)–C(34)	1.32 (1)		Rh–N(8)–C(38)	120.9 (8)	
N(7)–C(38)	1.32 (1)		Rh–N(8)–C(39)	118.9 (8)	
N(8)–C(38)	1.33 (1)		C(38)–N(8)–C(39)	119.8 (9)	
N(8)–C(39)	1.45 (1)		Rh–N(9)–C(45)	173.4 (9)	
N(9)–C(45)	1.13 (1)		N(1)–C(5)–N(2)	115 (1)	118.0 (4)
			N(3)–C(16)–N(4)	116 (1)	118.0 (4)
			N(5)–C(27)–N(6)	118 (1)	
			N(7)–C(38)–N(8)	118 (1)	
			C(46)–C(45)–N(9)	178 (1)	

adduct the Rh–N distance was 2.09 Å.

Results and Discussion

Syntheses and Molecular Structures. Two methods are generally used to prepare dinuclear rhodium complexes. Method 1 involves the reduction of a Rh(III) salt, usually $RhCl_3 \cdot 3H_2O$, in the presence of an anion with the correct orbital symmetry to bridge two rhodium ions. Method 2 involves the exchange of the bridging ligands of a $Rh_2(L)_4$ complex, usually $Rh_2(OOCCH_3)_4$, by heating the dimer complex in a melt of the ligand to be added. In this study both methods were employed to prepare 2-anilinopyridinate-bridged dirhodium complexes, and the two methods resulted in geometrically different major products.

The $Rh_2(ap)_4$ complex has four possible geometric isomers. The major product isolated by using method 1 is the trans isomer (**1**), which has a similar UV–vis spectrum and similar redox potentials as the $Rh_2(ap)_4$ complex reported by Tocher and Tocher.[1] However, a detailed study of the isolated $Rh_2(ap)_4$ shows that the UV–vis spectrum reported by Tocher and Tocher is that of a mixture of **1** in its reduced and oxidized forms (vide infra).

The selected bond distances and angles for **1b** are listed in Table II. A labeled ORTEP diagram of the molecule is presented in Figure 1a. The Rh–Rh bond distance of 2.412 Å falls within the expected range for dirhodium(II) complexes. The average Rh–N_p and Rh–N_a bond distances are 2.035 and 2.041 Å, respectively, and are essentially the same as those reported for $Rh_2(dpb)_4$.[3] A 14.3° average torsional twist of the equatorial planes of the two rhodium ions was observed for the complex.

Compound **2a** was isolated as the major product from the reaction mixture when method 2 was used for the synthesis and isolated as a minor product in the synthesis using method 1. The complex is a mixed-valent radical cation with a chloride counterion, $Rh_2(ap)_4Cl$. The selected bond distances and angles are listed in Table II. A labeled ORTEP diagram of the molecule is shown in Figure 1b. The prominent feature of the structure is the arrangement of the bridging ions such that all four pyridyl nitrogens are bound to one rhodium, Rh(1), with an average Rh–N_p distance of 2.048 Å. The second rhodium Rh(2) is bound equatorially to four anilino nitrogens with an average Rh–N_a bond distance of 2.008 Å. The Rh–Rh and Rh–Cl bond distances are 2.406 and 2.421 Å. A large average torsional angle of 23.4° was found.

Although there appear to be few differences between the average bond lengths mentioned above for both compounds, there are actually a few subtle distinctions. The Rh–Rh bond distances are virtually identical, which is surprising given the differences in cation charge and axial ligand type. The most obvious conclusion is that the forces involved which would tend to change the distance have been offset by a concomitant change in the torsion angle between the two equatorial rhodium planes and by the presence of a formal axial Cl^- bond in **2a**. No doubt, part of the large difference in the torsion angle must be due to the fact that **1b** is a (2,2-trans) isomer while **2a** is a (4,0) isomer. Thus, steric interference between neighboring phenyl rings has been minimized in **1b** and maximized in **2a**. Such a large torsional twist in **2a** also rotates the ortho hydrogens of the pyridyl groups and facilitates accommodation of the chloride ion at the axial site. At the opposite crowded end of the dimer the phenyl rings adopt mutual "edge-to-face" orientations, such that the ortho hydrogen of one phenyl group points toward the aromatic π cloud of its neighboring phenyl group. This same arrangement is found in $Rh_2(dpb)_4$, which still is able to form monoadducts with small, linear molecules such as CH_3CN and CO.[3] In the case of **2a**, however, the lack of substituent bulk at the $(N_p)_4$ end of the dimer makes this the preferred site for axial ligation.

Careful analysis of **1b** also shows some indication of steric strain due to the axial benzonitrile. As can be seen in Figure 1a, the phenyl rings on N(2) and N(6) "face" the axial ligand in order to minimize steric repulsion; however, the Rh(1)–N(2) and Rh(1)–N(6) lengths average 2.064 Å, whereas the Rh(2)–N(4) and Rh(2)–N(8) lengths average 2.019 Å. The latter value is essentially the same as the 2.008 Å found in **2a**, and therefore it is apparent that there must be some steric interference with the axial ligand causing lengthening of the Rh–N_a bonds. A change in electron density on the axially ligated rhodium is probably not involved since the Rh(1)–N_p bond lengths average 2.032 Å, essentially the same as the Rh(2)–N_p bond length average of 2.038 Å. Additional evidence of steric strain can be seen in the distances to the N_a atoms attached to Rh(1). N_a–C(Ph) averages 1.47 Å and N_a–C(py) averages 1.35 Å, considerably longer than their counterparts at Rh(2) (1.43 and 1.31 Å).

(10) Cotton, F. A.; De Boer, B. G.; La Prade, M. D.; Pipal, J. R.; Ucko, A. D. *Acta Crystallogr., Sect. B* **1971**, *B27*, 1664.

Table III. Half-Wave Potentials (V vs SCE) of the Dirhodium Complexes and ESR Data of the $Rh^{II}Rh^{III}$ Species in CH_2Cl_2, 0.1 M TBAP

compd (isomer)	added ligand	electrochem $E_{1/2}$	electrochem $E_{1/2}$[a]	ESR g_1	g_2	g_3 (10^4A_3, cm^{-1})	$g_\perp$	$g_\parallel$ ($10^4A_\parallel$, cm^{-1})
$Rh_2(ap)_4$ (**1**)		0.82	0.08	2.08	2.06	1.96 (15.6)		
(2,2 trans)	1 equiv of Cl^-	0.62	−0.18 (E_{pc}) 0.04 (E_{pa})	2.08	2.06	1.96 (15.6)		
	36 equiv of Cl^-	0.43	−0.18	2.07	2.05	1.95 (17.3)		
	1 equiv of CN^-	0.62	−0.30					
	2 equiv of CN^-	0.62	−0.30	2.09	2.07	1.93 (18.0)		
	1 atm of CO	0.80	0.25					
	10 equiv of CH_3CN	0.92	0.15	2.07	2.05	1.96 (17.4)		
$Rh_2(ap)_4Cl$ (**2a**)		0.52	−0.38				2.09	1.95 (26.4)
(4,0)	24 equiv of Cl^-	0.53	−0.38				2.10	1.95 (27.3)
	2 equiv of CN^-	0.52	−0.38				2.12	1.94 (29.0)
	1 atm of CO	0.52	−0.36 (E_{pc}) −0.12 (E_{pa})					
$Rh_2(ap)_4(CO)$[b] (4,0)	1 atm of CO	0.69	−0.17					

[a] Values of $E_{1/2}$ are oxidation potentials for **1** and reduction potentials for **2**. [b] Compound generated by controlled-potential reduction of **2a** under CO (see text). Both electrode reactions are electrooxidations.

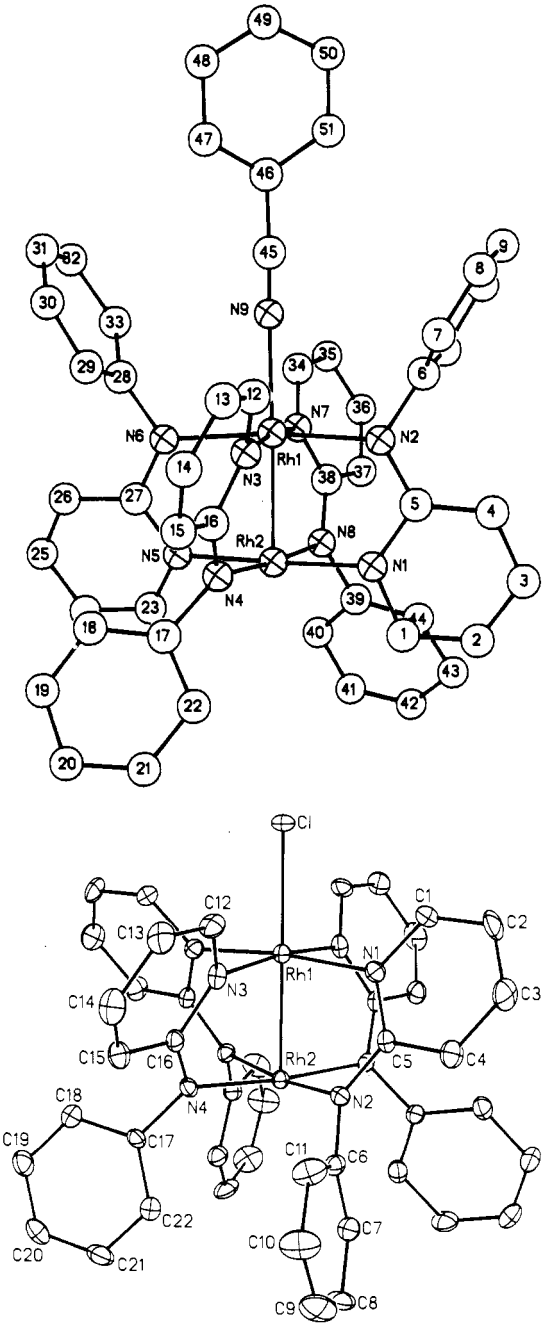

Figure 1. ORTEP diagrams of (a, top) $Rh_2(ap)_4(PhCN)$ (**1b**) and (b, bottom) $Rh_2(ap)_4Cl$ (**2a**).

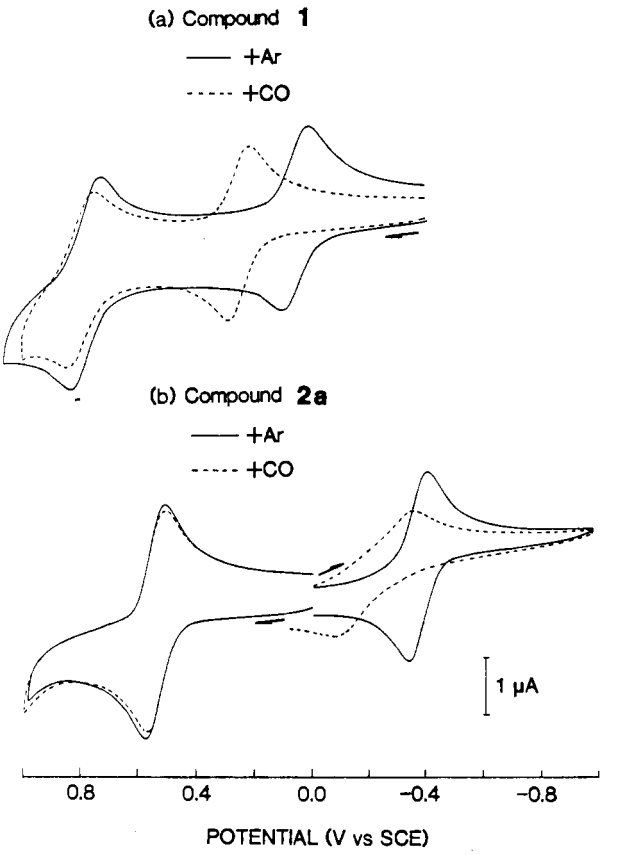

Figure 2. Cyclic voltammograms of (a) 8.0×10^{-4} M $Rh_2(ap)_4$ (**1**) and (b) 7.4×10^{-4} M $Rh_2(ap)_4Cl$ (**2a**) under argon (—) and under CO(---) in CH_2Cl_2, 0.1 M TBAP. Scan rate = 0.1 V/s.

The question regarding the relationship between the synthetic method used and geometric isomer produced needs to be addressed. First, it should be noted that the yields of the subject complexes are relatively low by both methods of synthesis. Therefore, a complex mixture of other rhodium-containing compounds is formed by both methods. Also, the 2-anilinopyridine ligand can interact with the rhodium dimer unit in various fashions. It can be monodentate, chelate to form a four-membered ring, bridge two metal centers, or undergo coordination via orthometalation.[11] We can only say that the isomers reported in this paper are the major products. A detailed study involving the isolation and characterization of all the complexes produced by the two methods described has not been attempted at this time.

(11) Chakravarty, A. R.; Cotton, F. A.; Tocher, D. A. *Organometallics* **1985**, *4*, 863.

Electrochemical Studies. Cyclic voltammograms of **1** and **2a** in dichloromethane under Ar and CO are shown in Figure 2, and half-wave potentials for the two redox processes of both complexes under various solution conditions are listed in Table III.

The cyclic voltammogram of **1** in CH_2Cl_2, 0.5 M $(TBA)BF_4$ has been characterized as undergoing two one-electron oxidation processes at $E_{1/2} = -0.01$ and $+0.64$V vs Ag/AgCl.[1] The values of $E_{1/2}$ in our study are somewhat shifted from the above values, probably due to differences in the experimental conditions. However, the molecular structure was not determined for the complex voltammetrically characterized in the literature, and we cannot rule out the possibility that complex **1** is a geometric isomer different from that which has been previously characterized.

The two oxidations of **1** correspond to reactions 1 and 2 under Ar in a nonbonding solvent such as CH_2Cl_2. The half-wave

$$Rh_2(ap)_4 \rightarrow [Rh_2(ap)_4]^+ + e^- \quad (1)$$

$$[Rh_2(ap)_4]^+ \rightarrow [Rh_2(ap)_4]^{2+} + e^- \quad (2)$$

potentials for reactions 1 and 2 are located at $E_{1/2} = 0.08$ and 0.82 V in CH_2Cl_2, 0.1 M TBAP, respectively. Values of $|E_{pa} - E_{pc}|$ vary between 60 and 70 mV at a scan rate of 0.2 V/s, while $i_{pa}/i_{pc} = 1$ and $i_p/v^{1/2}$ are invariant with increasing sweep rate, indicating that these are diffusion-controlled one-electron transfer processes.

The electrochemistry of **2a** under Ar is characterized by a reversible one-electron reduction at $E_{1/2} = -0.38$ V and a reversible one-electron oxidation at $E_{1/2} = 0.52$ V in CH_2Cl_2, 0.1 M TBAP. These values for **2a** are shifted cathodically by 300–460 mV compared to $E_{1/2}$ values for **1** under the same experimental conditions (see Table III). The more negative potentials of **2a** result from the different bonding arrangement of the bridging ligands (isomer effect) and the presence of the axially bound chloride ion (**1** contains no axial Rh–Cl bond).

The first oxidation potential for **1** under CO shifts anodically by 170 mV due to the formation of $Rh_2(ap)_4(CO)$. The second oxidation of **1** is insensitive to the presence of CO (see Figure 2a, dashed line). The CO dissociation rate from **1** is very slow in nonbonding solvents, and when the CO atmosphere is replaced by passing Ar through the solution, a significant amount of the CO adduct still remains even after 24 h.

The reduction of **2a** becomes irreversible in the presence of 1 atm of CO and is characterized by an $E_{pc} = -0.36$ V and an $E_{pa} = -0.12$ V (Figure 2b, dashed line). It thus appears that the reduction of **2a** is followed by Cl^- dissociation and a subsequent binding of CO. The $Rh^{II}_2(CO)$ adduct is then reoxidized at −0.12 V. No shift is observed in the first oxidation potential of $Rh^{II}Rh^{III}$, indicating that CO does not replace Cl^- in the neutral $Rh_2(ap)_4Cl$ complex. Different results are obtained in the absence of the chloride ion. For example, an electroreduction of **2a** in CH_2Cl_2 followed by bubbling CO gas through the solution leads to precipitation of $Rh_2(ap)_4(CO)$, which can be readily isolated. The $Rh_2(ap)_4(CO)$ compound is only slightly soluble in CH_2Cl_2 and the cyclic voltammogram of the complex in this solvent reveals two reversible oxidations at $E_{1/2} = -0.17$ and 0.69 V, corresponding to the oxidation of $Rh_2(ap)_4(CO)$ and $[Rh_2(ap)_4(CO)]^+$, respectively. The singly and doubly oxidized CO complexes are stable only on the cyclic voltammetry time scale, and a loss of CO occurs during controlled-potential oxidation of the complex.

The CO stretching frequencies for the CO adducts of **1** and **2** are 2048 and 2030 cm^{-1}, respectively, compared to 2143 cm^{-1} for free CO. The infrared data suggest that **2** is a better π donor than **1**, yet a larger anodic shift is found for the redox potential of **1** upon CO adduct formation. This could be due to **1** forming a CO bisadduct whereas **2** forms only a monoadduct. The CO stretches for all reported dirhodium(II) tetraamidate,[12] tetrathiocaprolactamate,[13] and tetraamidinate[4,14] complexes fall in the range 2004–2048 cm^{-1}, but there is not a clear correlation between the CO stretching frequency and the magnitude of $\Delta E_{1/2}$ for the $Rh^{II}Rh^{II}/Rh^{II}Rh^{III}$ redox couple of the CO bound and unbound complexes. However, an anodic shift of $E_{1/2}$ is always observed upon CO binding, indicating a decrease in metal-centered electron density as a result of rhodium to CO π back-bonding.

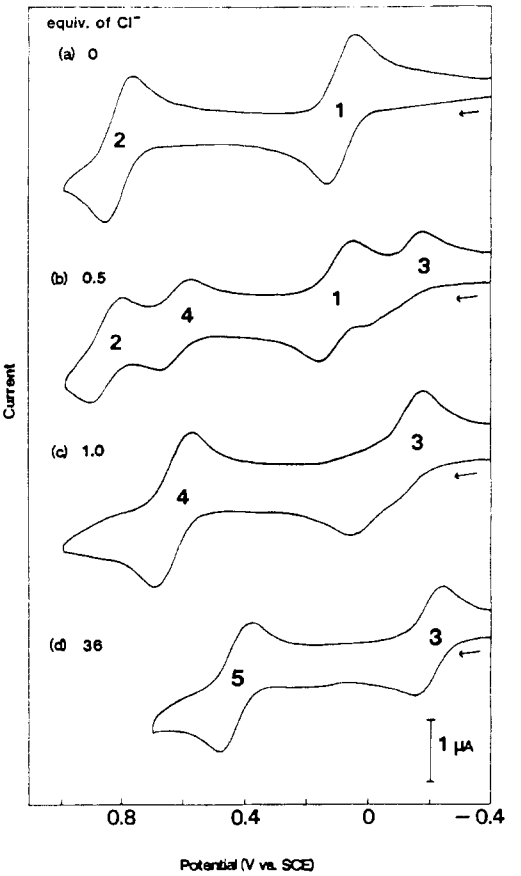

Figure 3. Cyclic voltammograms of 9.2×10^{-4} M $Rh_2(ap)_4$ (**1**) in CH_2Cl_2, 0.1 M TBAP with (a) 0, (b) 0.5, (c) 1.0, and (d) 36 equiv of (TBA)Cl. Scan rate = 0.1 V/s.

The coordination of Cl^- or CN^- to **1** and **2a** was monitored by cyclic voltammetry in order to determine the relative effects of anion axial binding and equatorial ligand bonding arrangements on the individual redox potentials. Solutions of **1** and **2a** in CH_2Cl_2, 0.1 M TBAP were titrated with CH_2Cl_2 solutions containing either (TBA)Cl or (TBA)CN, and the cyclic voltammograms then recorded. The addition of (TBA)Cl or (TBA)CN to **2a** had no effect on either of the redox potentials even at high concentrations. This suggests that Cl^- dissociation from $Rh_2(ap)_4Cl$ (**2a**) is slow and that a Cl^- bisadduct does not form in solution.

A different result is obtained during the titration of **1** with Cl^- or CN^-. Compound **1** undergoes reversible oxidations at $E_{1/2} = 0.08$ and 0.82 V in CH_2Cl_2 (waves 1 and 2, Figure 3a). However, upon the addition of (TBA)Cl to this solution, both waves decrease in intensity and two new waves (waves 3 and 4) begin to appear (see Figure 3). One wave involves a reversible oxidation at $E_{1/2} = 0.62$ V (wave 4), and the other, an irreversible reduction at $E_p = -0.18$ V (wave 3). No anodic wave is coupled to the cathodic potential of wave 3 in CH_2Cl_2 solutions containing up to 1 equiv of Cl^-. This indicates that compound **1** does not bind to Cl^- at a $Cl^-/Rh_2(ap)_4$ ratio less than 1. However, upon oxidation of **1**, $Rh_2(ap)_4Cl$ is formed in solution. This compound is reversibly oxidized at 0.62 V (wave 4, Figure 3b,c) and irreversibly reduced at −0.18 V (wave 3, Figure 3b,c). The latter reaction is followed by a Cl^- dissociation, and therefore no corresponding anodic wave is coupled to the reduction process 3. The anodic peak of process

(12) Chavan, M. Y.; Ahsan, M. Q.; Lifsey, R. S.; Bear, J. L.; Kadish, K. M. *Inorg. Chem.* **1986**, *25*, 3218.
(13) Lifsey, R. S.; Chavan, M. Y.; Ahsan, M. Q.; Kadish, K. M.; Bear, J. L. *Inorg. Chem.* **1987**, *26*, 822.
(14) Narris, M. Ph.D. Dissertation, University of Houston, 1986.

Scheme I. Electron-Transfer Reactions of **1** in the Presence and Absence of Cl^-

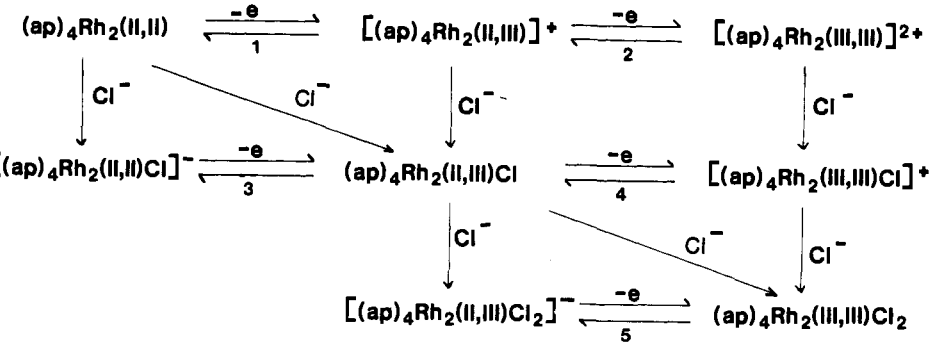

1 shifts cathodically as Cl^- is added to the solution and is observed at $E_p = 0.04$ V when the $Cl^-/Rh_2(ap)_4$ ratio is equal to 1.0. Under these conditions the electrode reaction corresponds to the reoxidation of $Rh_2(ap)_4$.

When the $Cl^-/Rh_2(ap)_4$ ratio is greater than 1.0, wave 3 gradually becomes reversible, while the reversible second oxidation at $E_{1/2} = 0.62$ V shifts in a cathodic direction. Wave 3 becomes totally reversible at 36 equiv of Cl^- (see Figure 3d). A plot of $E_{1/2}$ for the second oxidation of $Rh_2(ap)_4Cl$ (wave 5) vs log $[Cl^-]$ over the range 1.0–200 equiv of Cl^- gives a slope of −65 mV, while the $E_{1/2}$ of wave 3 is not a function of the Cl^- concentration. This indicates that one Cl^- is bound to **1** at high $[Cl^-]$ and that the process at $E_{1/2} = -0.18$ V can be written as shown in reaction 3.

$$[Rh_2(ap)_4Cl]^- \rightarrow Rh_2(ap)_4Cl + e^- \quad (3)$$

The second oxidation of $Rh_2(ap)_4Cl$ is followed by formation of the chloride bisadduct to form $Rh_2(ap)_4Cl_2$, and the reaction occurs as written in reaction 4. Combining the results from the elec-

$$Rh_2(ap)_4Cl + Cl^- \rightarrow Rh_2(ap)_4Cl_2 + e^- \quad (4)$$

tron-transfer processes and the ligand addition/exchange reaction leads to the mechanism shown in Scheme I for the oxidation reaction of compound **1**. The numbers in this scheme correspond to the processes illustrated in the voltammograms of Figure 3.

Similar types of reactions occur in the presence of CN^- ion. When up to 1.5 equiv of CN^- is added to a CH_2Cl_2 solution containing 9.0×10^{-4} M $Rh_2(ap)_4$, two new waves are again observed at $E_{1/2} = -0.30$ and 0.62 V (see Figure 4a–c). Unlike results from the chloride titration, both new processes involve reversible oxidations, indicating that the binding constant of **1** with CN^- is much larger than the binding constant with Cl^-.

The first oxidation potential of $[Rh_2(ap)_4CN]^-$ is at $E_{1/2} = -0.30$ V, which is 100 mV cathodically shifted from that of the chloride adduct, $[Rh_2(ap)_4Cl]^-$. The second oxidation potential of both complexes is at $E_{1/2} = 0.62$ V (see Figure 4a–c). However, when more than 1.5 equiv of CN^- is added to the solution of $[Rh_2(ap)_4CN]^-$, the oxidation wave at −0.30 V does not change, while the reversible second oxidation at +0.62 V is gradually replaced by an irreversible oxidation at $E_p = +0.42$ V (Figure 4d). (TBA)CN in CH_2Cl_2 has an irreversible oxidation wave at $E_p \approx +0.4$ V, and this indicates that the irreversible oxidation at $E_p = +0.42$ V in Figure 4d is due to a direct oxidation of free CN^- ions from the (TBA)CN added to the solution. This oxidation of free CN^- poisoned the Pt electrode. Thus, even though bisadducts of singly and doubly oxidized **1** are probably formed, we were unable to electrochemically characterize these complexes.

The above data indicate that axial binding by CO stabilizes the Rh^{II}_2 oxidation state. This positive shift in oxidation potentials results from the donation of π-electron density from the filled Rh–Rh π* orbitals to the antibonding π* orbitals of CO. A different effect is observed for complexes bound with the anions Cl^- or CN^-. In this case axial binding to either anion stabilizes the higher oxidation states of the dimeric unit. CN^- ion, which can function as a σ donor and π acceptor, axially binds to both the neutral and oxidized forms of the two geometric isomers.

Spectroscopic Studies. Figure 5 shows the electronic absorption spectra of both isomers in their Rh^{II}_2 oxidation state (solid line)

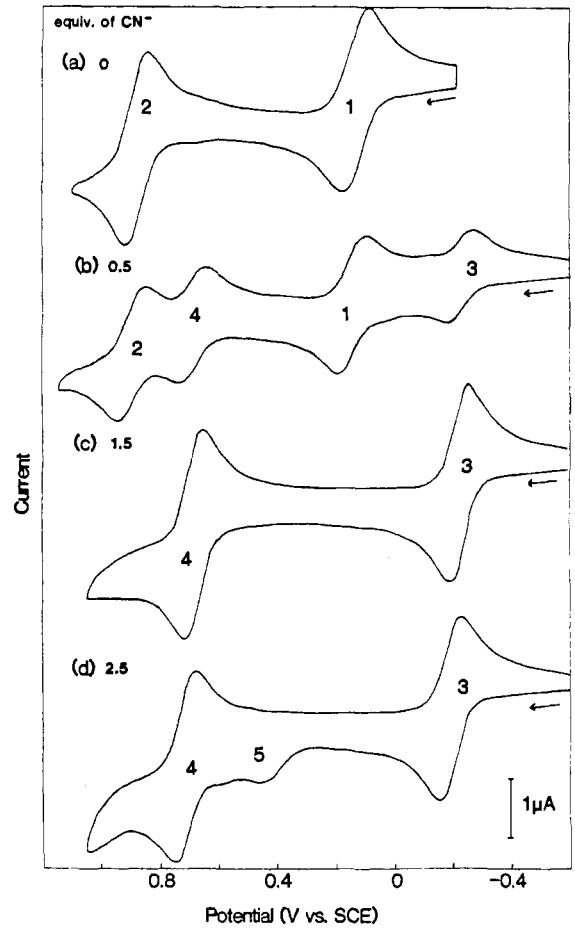

Figure 4. Cyclic voltammograms of 9.0×10^{-4} M $Rh_2(ap)_4$ (**1**) in CH_2Cl_2, 0.1 M TBAP with (a) 0, (b) 0.5, (c) 1.5, and (d) 2.5 equiv of (TBA)CN.

and $Rh^{II}Rh^{III}$ oxidation state (dashed line). Complexes **1** and **2** in the Rh^{II}_2 oxidation state do not display any strong absorption peak above 600 nm (solid lines, Figure 5). The broad weak absorptions observed in the regions from 800 to 1600 nm for compound **1** and from 700 to 2000 nm for compound **2** are due to trace amounts of the singly oxidized complexes. The high molar absorptivity of these near-IR bands and the easy oxidation of both complexes make it difficult to obtain totally pure Rh^{II}_2 complexes.

The spectrum reported by Tocher and Tocher[1] has a large absorbance between 800 and 1600 nm, indicating that a relatively high concentration of the singly oxidized complex was present in their sample. When **1** is singly oxidized, a broad strong absorption is observed in the near-IR region with the peak maximium located near 1045 nm ($\epsilon = 6.1 \times 10^3$ and a shoulder around 1470 nm ($\epsilon = 1.5 \times 10^3$) (dashed line, Figure 5a). Compound **2a** shows strong absorption at 910 nm ($\epsilon = 5.1 \times 10^3$) and 1530 nm ($\epsilon = 3.8 \times 10^3$) (dashed line, Figure 5b). These near-IR bands are most probably nitrogen-to-metal charge-transfer transitions involving

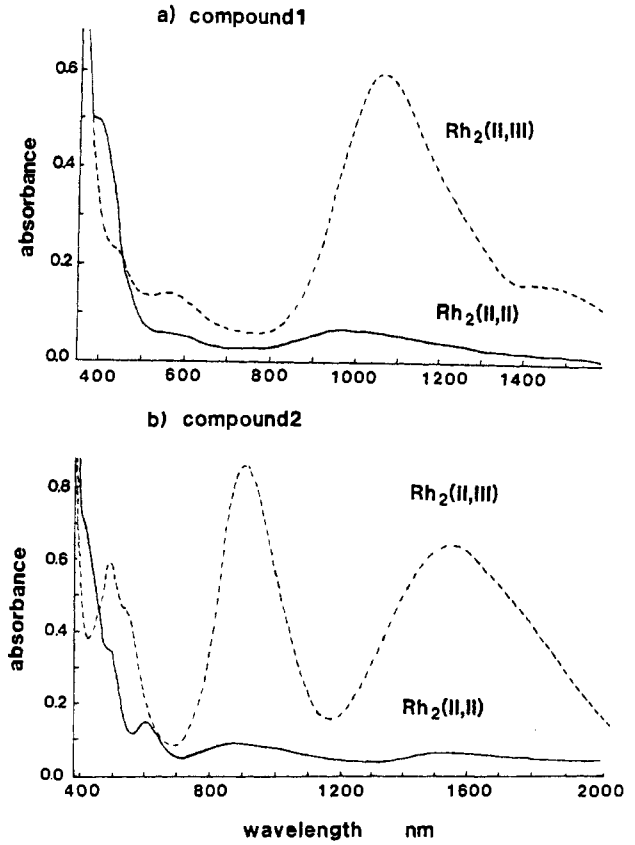

Figure 5. Electronic absorption spectra of $Rh_2(ap)_4$ complexes in CH_2Cl_2: (a) **1** (—) and singly oxidized **1** (---); (b) **2a** (---) and singly reduced **2a** (—).

two of the filled nitrogen π nonbonding molecular orbitals and the partially filled rhodium-centered HOMO. The low energy of these transitions shows that the nitrogen nonbonding π orbitals are very close in energy to the singly occupied molecular orbital (SOMO). In fact, an irreversible oxidation of $[Rh_2(ap)_4]^{2+}$ occurs at 1.25 V at a scan rate 0.1 V/s, resulting in decomposition of the complex.

A preliminary ESR study of **1a** and **2a** has been reported in an earlier communication.[2] Figure 6 illustrates the ESR spectra for the radical cation of the two geometric isomers in CH_2Cl_2 with and without CN^- ion at 77 K. The g values in different solvents and with different counterions in frozen glass are listed in Table III.

Compound **1a** gives a rhombic ESR signal in both CH_2Cl_2 and CH_3CN at 77 K with g_3 split into a 1:2:1 triplet. These results are consistent with the odd-electron orbital being equally distributed on both rhodium centers. The g values and $A_\parallel$ values are relatively insensitive to the nature of the counterion. This is true even though the σ-donor ability of the counterions used (ClO_4^-, Cl^-, and CN^-) varies over a wide range.

Compound **2a** gives an axial ESR spectrum in bonding and nonbonding solvents with $g_\parallel$ split into a doublet and is the first example of a $Rh^{II}Rh^{III}$ complex where the odd electron is localized on one rhodium ion. Also, the value of $A_\parallel$ is greater for **2a** than for **1a**. It is interesting to note that an axial ESR spectrum is observed for compound **2a**, while the spectrum of compound **1a** gives a rhombic signal. The exact reason for this phenomenon is not clear at present. Two axial ligation sites of compound **1a** have the same steric environment, and for this reason there is a strong possibility of forming bisadducts in solution, whereas for compound **2a** the axial and equatorial ligand environments are different for the two rhodium ions of the dimer unit. We underscore the fact that all of the structural and electrochemical data for **2** in its reduced and singly oxidized states indicate the presence of exclusive monoadduct formation. The key questions then are, What is the nature of the SOMO in $[Rh_2(ap)_4]^+$ and why does it become strongly polarized on one atom?

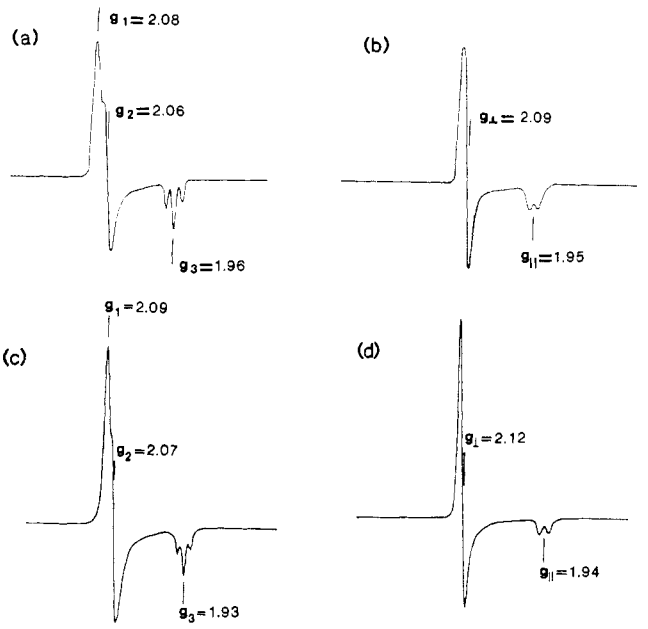

Figure 6. ESR spectra of frozen-glass solutions: (a) singly oxidized **1**, $[Rh_2(ap)_4]^+$ in CH_2Cl_2, 0.1 M TBAP; (b) **2a** in CH_2Cl_2, 0.1 M TBAP; (c) solution a with 2 equiv of (TBA)CN; (d) solution b with 2 equiv of (TBA)CN.

Extended Hückel Calculations. There have been a number of theoretical studies on dirhodium tetracarboxylates and their radical cations.[15-25] Most have agreed on a $\sigma^2\pi^4\delta^2\pi^{*4}\delta^{*2}$ level ordering for $Rh_2(O_2CH)_4$. In some cases π^* has been found to be the HOMO; however, the energy difference between π^* and δ^* in all treatments is quite small. Photoelectron spectroscopy and ab initio calculations[26] on $Rh_2(mhp)_4$ (mhp = 2-hydroxy-6-methylpyridinate), as well as $Rh_2(form)_4$,[27] have been used to establish the same level ordering. This sequence is also found in most studies for $Rh_2(O_2CH)_4L_2$ when L is a weak σ donor (e.g. H_2O). In the radical cation there is a small energy difference between the $\sigma^2\pi^4\delta^2\delta^{*2}\pi^{*3}$ and $\sigma^2\pi^4\delta^2\pi^{*4}\delta^{*1}$ states. The most recent calculations[25] on $[Rh_2(O_2CH)_4(H_2O)_2]^+$ put the former as the ground state with the latter at 0.3 eV higher in energy, although this remains controversial.[17,21] When L is a strong σ donor (e.g., PR_3), the σ level is destabilized and becomes the HOMO.[20-22] Thus, the ground-state configuration of $[Rh_2(O_2CH)_4(PH_3)_2]^+$ is predicted to be $\pi^4\delta^2\pi^{*4}\delta^{*2}\sigma^1$, and there is some experimental support for this hypothesis.[20,28] The ground states for the rhodium dimer cations that contain bridging ligands other than carboxylates are more uncertain. The behavior of the ESR spectra for $[Rh_2(OAc)_n(acam)_{4-n}L_2]^+$ (OAc = acetate, acam = acetamidate) where n = 0–4 is compatible with a change of the ground state

(15) Dubicki, L.; Martin, R. *Inorg. Chem.* **1970**, *9*, 673.
(16) Norman, J. G.; Kolari, H. J. *J. Am. Chem. Soc.* **1978**, *100*, 791.
(17) Norman, J. G.; Renzoni, G. E.; Case, D. A. *J. Am. Chem. Soc.* **1979**, *101*, 5256.
(18) Nakatsuji, H.; Ushio, J.; Kanda, K.; Onishi, Y.; Kawamura, T.; Yonezawa, T. *Chem. Phys. Lett.* **1981**, *79*, 299.
(19) Kawamura, T.; Katayama, H.; Yamabe, T. *Chem. Phys. Lett.* **1986**, *130*, 20.
(20) Sowa, T.; Kawamura, T.; Shida, T.; Yonezawa, T. *Inorg. Chem.* **1983**, *22*, 56.
(21) Nakatsuji, H.; Onishi, Y.; Ushio, J.; Yonezawa, T. *Inorg. Chem.* **1983**, *22*, 1623.
(22) Bursten, B. E.; Cotton, F. A. *Inorg. Chem.* **1981**, *20*, 3042.
(23) Drago, R. S.; Tanner, S. P.; Richmann, R. M.; Long, J. R. *J. Am. Chem. Soc.* **1979**, *101*, 2897.
(24) Drago, R. S.; Long, J. R.; Casmano, R. *Inorg. Chem.* **1982**, *21*, 2196.
(25) Mougenot, P.; Demuynck, J.; Benard, M. *Chem. Phys. Lett.* **1987**, *136*, 279.
(26) Berry, M.; Garner, C. D.; Hillier, I. H.; McDowell, A. A.; Clegg, W. *J. Chem. Soc., Chem. Commun.* **1980**, 494.
(27) Rizzi, G. A.; Casarin, M.; Tondello, E.; Piraino, P.; Granozzi, G. *Inorg. Chem.* **1987**, *26*, 3406.
(28) Kawamura, T.; Fakamachi, K.; Sowa, T.; Hayashida, S.; Yonezawa, T. *J. Am. Chem. Soc.* **1981**, *103*, 364. Hayashida, S.; Kawamura, T.; Yonezawa, T. *Inorg. Chem.* **1982**, *21*, 2235.

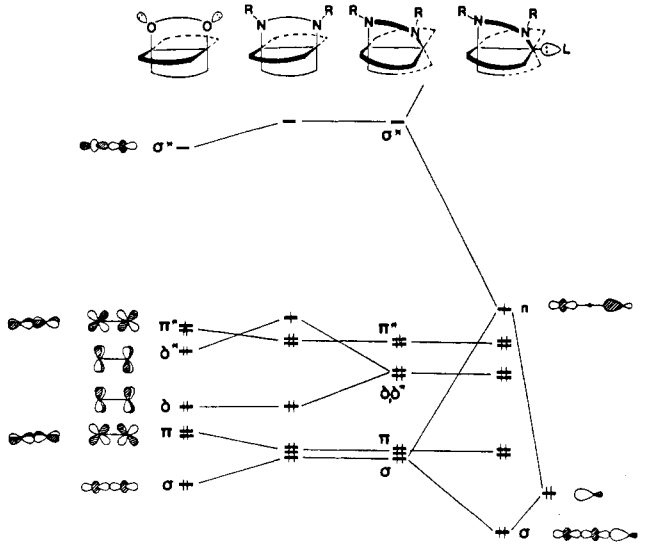

Figure 7. Molecular orbital pattern for acetate and amidinate complexes.

from $...\pi^{*4}\delta^{*1}$ to $...\delta^{*2}\pi^{*3}$ when n changes from 3 to 4. These data again support a small energy difference between the two states.[17,21,29]

For **1a** and the amidinate-bridged complexes, $[Rh_2(dpb)_4]^+$, $[Rh_2(form)_4]^+$, and $[Rh_2(dpf)_4]^+$ (dpf = *N,N'*-diphenylformamidinate), $g_\parallel$ is split into a 1:2:1 triplet *in a nonbonding solvent*.[3,4,30] The latter three compounds form monoadducts (e.g. CH_3CN, CO, and Cl^-), and $g_\parallel$ is split into a 1:1:1:1 doublet of doublets. Thus, the SOMO is polarized toward one rhodium atom. For $[Rh^{II}Rh^{III}(dpb)_4L]^+$ the difference in $A_\parallel$ of the two rhodium ions roughly scales as a function of the σ-donor strength of L in the order: $CN^- > CO > SCN^- > Cl^- \sim CH_3CN$.[14] Finally, the doublet observed for $g_\parallel$ for **2a** implies localization of the SOMO on one rhodium atom. There are two basic mechanisms that can be used to explain the polarization of electron density in the SOMO.

Localized hole states have been found for $[Rh_2(O_2CH)_4(H_2O)_2]^+$.[25] However, it is not clear whether delocalized or localized solutions will be more stable with large CI expansions. In the present context, the presence of one axial ligand could in principle induce a polarization or localization of a δ* (or π*) hole state solely on electrostatic grounds. We do not favor this hypothesis, since $g_\parallel$'s in both $[Rh_2(OAc)(acam)_3L_2]^+$ and $[Rh_2(OAc)_3(acam)L_2]^+$ are triplets. In both cases the equatorial environment should provide a more significant impact on the δ* or π* hole states than perturbation by an axial ligand.

The two mechanisms that we favor rely on the polarization of the electron density of the σ system by one axial ligand. The left side of Figure 7 shows the results of our extended Hückel calculations on $[Rh_2(O_2CH)_4]^+$. The SOMO is predicted to be π* with δ* lying slightly below it in energy. On going to $[Rh_2((NH)_2CH)_4]^+$, the substitution of eight NH groups for oxygens causes the δ* and σ levels to be raised in energy, while π and π* are lowered. This results from the increased donor ability of the amidinate nitrogens and the absence of lone pairs on the oxygens that serve to destabilize π and π*. Not shown in Figure 7 is the uniform raising of all metal-based orbitals due to the lower electronegativity of nitrogen compared to oxygen. The important point, and this is also seen in the DV-Xα calculations on the two neutral molecules,[27] is that δ* now lies at a sizable energy above π* and that σ is close to π. In all of the reported structures of amidinate complexes there is significant twisting about the Rh–Rh axis. For example, the N–Rh–Rh–N torsion angle in $Rh_2(form)_4$ is 16.7°,[4] in $Rh_2(dpb)_4$ it is 17.3°,[3] in $Rh_2(dpf)_4(CH_3CN)$ it is 16.8°,[30] and finally in **2a** is 23.5°. This rotation around the Rh–Rh axis, which presumably is set by geometrical demands of the bridging ligands, will stabilize δ* and destabilize δ. Ultimately, at a 45° rotation angle δ and δ* become degenerate as shown in the middle of Figure 7.

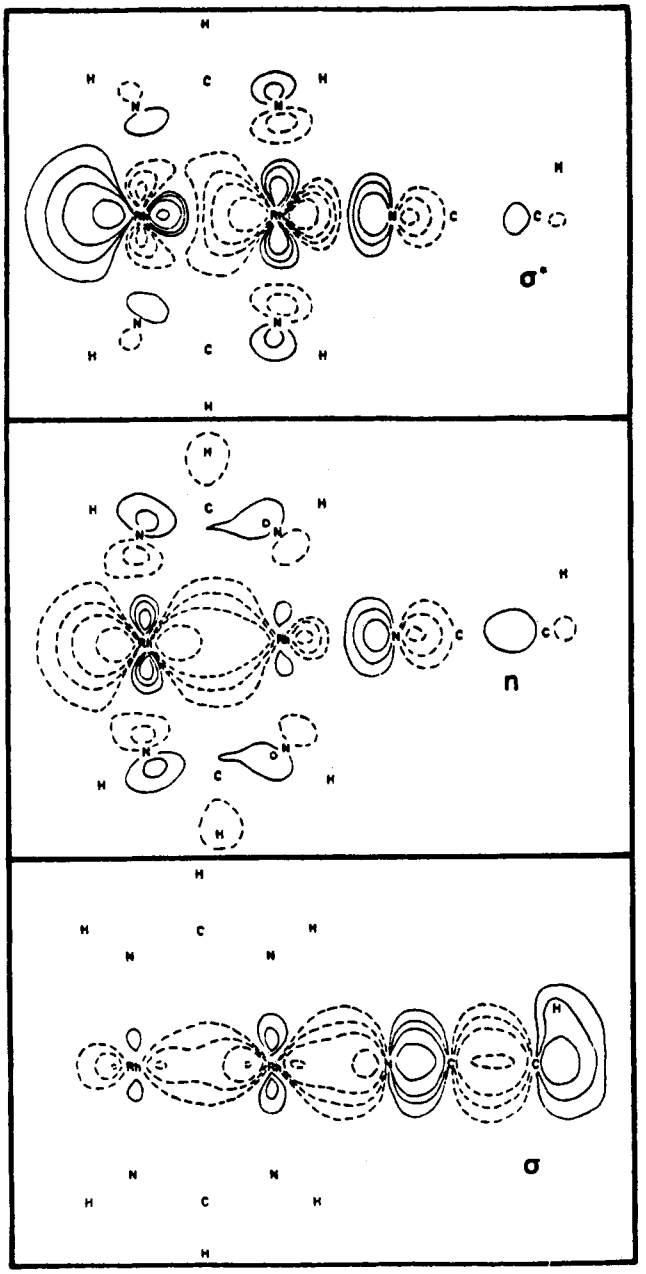

Figure 8. σ*, n, and σ molecular orbitals for $[Rh_2((NH)_2CH)_4(CH_3CN)]^+$. The contour values are ±0.03, ±0.06, ±0.10, and ±0.20.

An axial ligand's donor function, on the far right of Figure 7, will interact with σ and σ* to form a classical three-orbital problem.[31] The lowest molecular orbital, labeled σ, is localized on the axial ligand with Rh–Rh σ mixed in a bonding fashion. The middle level, labeled n, is predominantly Rh–Rh σ destabilized by the axial ligand. Most importantly, some Rh–Rh σ* mixes into this orbital in a bonding fashion to the axial donor function. This significantly decreases the amplitude of the axially coordinated rhodium atom. Finally, the highest energy molecular orbital, not shown in Figure 7, is primarily Rh–Rh σ* with the donor function mixed into it in an antibonding fashion. Contour plots of these molecular orbitals in $[Rh_2((NH)_2CH)_4(CH_3CN)]^+$ are presented in Figure 8. The polarization of n toward the uncoordinated rhodium atom is striking; 60.3% of the electron density is concentrated on this atom, while only 15.4% remains on the

(29) Chavan, M. Y.; Zhu, T. P.; Lin, X. Q.; Ahsan, M. Q.; Bear, J. L.; Kadish, K. M. *Inorg. Chem.* **1984**, *23*, 4538.

(30) Bear, J. L.; Lifsey, R. S.; Yao, C.-L. To be submitted for publication. Lifsey, R. S. Ph.D. Dissertation, University of Houston, 1987.

(31) Albright, T. A.; Burdett, J. K.; Whangbo, M. H. *Orbital Interaction in Chemistry*; Wiley: New York, 1985.

axially coordinated rhodium atom. An identical polarization for the same reason has recently been found at the ab initio SCF level for $[Rh_2(tcl)_4(CO)]^+$ (tcl = thiocaprolactamate).[32] Notice that there is some, albeit smaller, polarization in the σ and σ^* molecular orbitals. The direction of polarization can easily be established from perturbation theory considerations.[31] The simplest explanation then for the ESR behavior of the radical cation amidinate complexes is that the SOMO is n, as shown in Figure 7. This mechanism is sensitive to the σ-donor strength of the axial ligand and twisting around the Rh–Rh axis. The former effect serves to destabilize n; the latter stabilizes δ^*. It is also important to note that as the σ-donor strength of the axial ligand increases, the mixing of Rh–Rh σ^* into n increases and, hence, the polarization of electron density onto the uncoordinated rhodium increases.

The second explanation for the ESR behavior that we have observed utilizes spin polarization.[33] Let us presume that n lies below δ^* and π^*; its polarization toward the uncoordinated rhodium should create greater spin density on the coordinated rhodium atom. This agrees with the results of ab initio SCF/CI calculations[32] on $[Rh_2(tcl)_4(CO)]^+$ where the ... $n^2\pi^{*4}\delta^{*1}$ and $n^2\delta^{*2}\pi^{*3}$ states were found to be nearly degenerate and ~0.3 eV lower in energy than $\pi^{*4}\delta^{*2}n^1$. This energy difference, however, is certainly small enough so that the hole state in the present compounds is uncertain. For both mechanisms the introduction of a second axial ligand will destroy the asymmetry in n. Consistent with this is a titration study[30] of $[Rh_2(dpf)_4]^+$ with Cl^- and CN^-. As mentioned previously, with one axial ligand $g_{\parallel}$ is a doublet of doublets. When both ligands are added in large excess, the bisadduct is formed and $g_{\parallel}$ becomes a 1:2:1 triplet. We look forward to the results of more sophisticated calculations which hopefully will be able to differentiate between the two proposed mechanisms.

In summary, the two geometric isomers of $Rh_2(ap)_4$ display considerably different chemical and electrochemical properties. These differences appear to result from polarization of the electron density on the two metal centers of **2a**, stemming from the propensity of the complex to form monoadducts. The first oxidation potential of **2** is 460 mV more negative than $E_{1/2}$ for oxidation of **1** and reflects significant polarization even in the neutral $Rh^{II}Rh^{II}$ complex. In fact, the chemical and electrochemical behavior of **2** is somewhat like that expected for a $Rh^{I}Rh^{III}$ complex. There is no question that **2a** is a "true" mixed-valent $Rh^{II}Rh^{III}$ complex and to our knowledge is the only example of such a dinuclear rhodium complex. Even though **1b** crystallizes as the monoadduct, electrochemical studies show that **1** and **1a** form bisadducts in solution. In addition, the equatorial ligand symmetry and the steric constraint at the axial site of the two rhodium ions are the same. As a result, **1a** shows little tendency toward axial polarization. There are still unanswered questions regarding the mechanism of polarization exhibited by **2a**, and the rich and diverse chemistry of these complexes warrants further study.

Acknowledgment. This work was supported by the Robert A. Welch Foundation (J.L.B., Grant No. E-918; K.M.K., Grant No. E-680; T.A.A., Grant No. E-705), the Petroleum Research Fund, administered by the American Chemical Society (T.A.A.), and the NSF via an allocation of computer time at the Pittsburgh Supercomputing Center.

Registry No. **1**, 99243-16-0; **1a**, 99243-17-1; **1b**, 109532-20-9; **2**, 119072-77-4; **2a**, 109532-21-0; $Rh_2(OOCCH_3)_4$, 15956-28-2; $[Rh_2(ap)_4]^{2+}$, 99243-18-2; $[Rh_2(ap)_4Cl]^-$ (4,0 isomer), 119072-91-2; $Rh_2(ap)_4(CO)$ (2,2-trans isomer), 119072-84-3; $[Rh_2(ap)_4(CO)]^+$ (2,2-trans isomer), 119111-94-3; $[Rh_2(ap)_4(CO)]^{2+}$ (2,2-trans isomer), 119072-85-4; $Rh_2(ap)_4(CO)$ (4,0 isomer), 116564-36-4; $[Rh_2(ap)_4(CO)]^+$ (4,0 isomer), 119072-89-8; $[Rh_2(ap)_4(CO)]^{2+}$ (4,0 isomer), 119072-90-1; $[Rh_2(ap)_4Cl]^-$ (2,2-trans isomer), 119072-78-5; $Rh_2(ap)_4Cl$ (2,2-trans isomer), 119072-83-2; $[Rh_2(ap)_4Cl]^+$ (2,2-trans isomer), 119072-79-6; $[Rh_2(ap)_4Cl_2]^-$, 119072-80-9; $Rh_2(ap)_4Cl_2$, 119072-81-0; $[Rh_2(ap)_4(CN)]^-$ (2,2-trans isomer), 119072-86-5; $Rh_2(ap)_4(CN)$ (2,2-trans isomer), 119072-87-6; $[Rh_2(ap)_4(CN)]^+$ (2,2-trans isomer), 119072-88-7; $[Rh_2(O_2CH)_4]^+$, 71767-77-6; $[Rh_2((NH)_2CH)_4]^+$, 119072-82-1; $[Rh_2((NH)_2CH)_4(CH_3CN)]^+$, 119111-93-2.

Supplementary Material Available: For **1b** and **2a**, Tables SI–SIV, listing data collection and processing parameters, positional parameters, hydrogen atomic coordinates, and anisotropic thermal parameters (5 pages); Tables SV and SVI, listing observed and calculated structure factors (36 pages). Ordering information is given on any current masthead page.

(32) Poblet, J. M.; Benard, M. *Inorg. Chem.* **1988**, *27*, 2935.

(33) See for example: Szabo, S.; Ostlund, N. S. *Modern Quantum Chemistry: Introduction to Advanced Electronic Structure Theory*; MacMillan: New York, 1982; pp 206–221. Salem, L. *Electronics in Chemical Reactions: First Principles*; Wiley: New York, 1982; pp 190–198.